

# Results from a new die-to-database reticle inspection platform

William H. Broadbent\*, James N. Wiley, Zain K. Saidin, Sterling G. Watson,  
David S. Alles, Larry S. Zurbrick, Chris A. Mack  
KLA-Tencor Corporation, 160 Rio Robles, San Jose, CA, USA 95134-1809

## ABSTRACT

A new DUV die-to-database high-resolution reticle defect inspection platform has been developed. This platform is designed to meet the 90nm through 65nm node 248/193nm lithography reticle qualification requirements of the IC industry. These design nodes typically include: COG layers, EPSM layers, and AltPSM layers, plus aggressive OPC which includes jogs, serifs, and SRAF (sub-resolution assist features). The architecture and technology of the new inspection platform is described. Die-to-database inspection results are shown on standard programmed defect test reticles, as well as, advanced 90nm through 65nm node reticles from industry sources. Results show high sensitivity and low false detections being achieved.

Keywords: DUV, 193nm, 248nm, reticle, defect, inspection, sensitivity, flux, OPC, SRAF

## 1. INTRODUCTION

The current generation of UV reticle defect inspection systems have provided excellent performance for current IC manufacturing through the 130nm node. Using high resolution imaging and UV wavelength illumination, these systems have been effective in finding critical reticle defects during reticle manufacturing, and further, finding critical reticle defects that occur during reticle use, thus protecting wafer fabs from catastrophic yield losses. UV illumination has been effective for both 365nm and 248nm wavelength wafer lithography.

These UV systems have been extended for use in the 90nm node, however, the lower  $k_1$  and 193 lithography of the 90nm node are demanding detection of smaller defects on smaller feature sizes, and challenging these systems. Furthermore, local CD defects, crystal type, and haze type defects have been problematic in some advanced wafer fabs. The recently developed DUV reticle inspection platform uses DUV illumination for higher imaging resolution, thus allowing inspection of smaller feature sizes, and detection of smaller defects. In addition, the DUV wavelength is providing better contrast to crystal, haze, and quartz phase defects thus providing an important sensitivity advantage.

The first available capability of this DUV platform was die-to-die inspection for the 90nm node using a 125nm pixel. The platform has now been extended to include transmitted light die-to-database inspection, a new 90nm pixel for the 65nm node, and further includes reflected illumination die-to-die inspection. Development is currently underway to give the platform additional capability including: reflected illumination die-to-database inspection, and STARlight™ contamination inspection. Thus, when completed, the platform will include the necessary inspection modes, illumination modes, and detection algorithms, suitable for the variety of extreme OPC and phase shifting techniques anticipated for the 65nm node.

Factory test results of the new capabilities are discussed. Several prototype systems, the KLA-Tencor standard test reticles, and a large set of industry provided reticles were used for the testing.

The system also includes a die-to-database implementation of the lithography oriented defect detectors originally developed for the die-to-die mode (Litho1 and Litho2). These detectors are designed to approximate wafer lithography conditions to favor the detection of lithography significant defects. Whereas, the standard high resolution detectors (HiRes1 and HiRes2) are designed to detect defects primarily based on their size without particular regard to their lithographic significance. The Litho2 detector is designed for high sensitivity of lithographically significant defects on contact and hole layers, while the Litho1 detector is designed primarily for line/space layers.

\* bill.broadbent@kla-tencor.com; voice 408-875-6153; fax 408-875-4262

STARlight is a trademark of KLA-Tencor Corporation

Litho1 further offers a second sub-detector with user-adjustable variable detection sensitivity according to the local mask enhancement factor (MEF), thus, defects in high MEF locations can be selected to be detected with very high sensitivity, whereas, defects in low MEF locations are detected with lower sensitivity. When used in conjunction with the traditional high resolution detectors, defects can be binned as either lithographically significant, or not lithographically significant. Test results for the high resolution and Litho2 detectors are discussed in this paper; test results for the Litho1 detector are not discussed.

## 2. DUV RETICLE INSPECTION DEVELOPMENT

KLA-Tencor is currently in active development of the DUV TeraScan platform. This advanced DUV platform currently includes a die-to-die inspection mode, it now includes a die-to-database mode, and it soon will include a STARlight™ contamination mode. The system is pictured in Figure 2-1 (database prep processor and image computer not shown). The original TeraScan 525 die-to-die model has been released and is currently in production use at several advanced reticle manufacturing sites. The TeraScan 576 die-to-database model is currently starting the beta testing cycle, while the STARlight capability is being designed.

The TeraScan platform continues KLA-Tencor's tradition of high resolution imaging for high performance reticle inspection. This technique uses significantly higher resolution imaging of the reticle than the wafer lithography system, thus allowing direct inspection of both the primary structures and the sub-resolution structures to ensure a high quality reticle. Furthermore, since the inspection is done at high resolution where actinic wavelength is less important, a single wavelength system can provide good performance inspecting reticles from a variety of lithographic wavelengths.



Figure 2-1: TeraScan 5xx DUV Reticle Inspection System

The traditional high resolution defect detectors find defects primarily based on their size with little regard for their context and lithographic significance. The recently developed Lithographic Detectors can be adjusted to favor defects with lithographic significance. These two classes of detectors can be used effectively together since different defects may be significant to different groups of reticle parties. By binning defects differently, the different reticle parties can concentrate on the defects of most interest. For instance, small defects on large geometry, or on sub-resolution assist features (SRAF), may have little lithographic significance since the MEF is low, so they may not be important to a lithographer. However, these defects can be important to the reticle manufacturer for process control as an indication of process quality. The high resolution detectors can be set to find and bin these defects, while the lithographic detectors may be set to not find these defects. This technique is effective since a high resolution inspection system has the ability to image many types of defects, and with the appropriate image processing, can bin different defect types appropriately. Both the traditional High Resolution defect detectors, and the Lithographic defect detectors are available in both the die-to-die and the die-to-database modes, and are planned for the STARlight mode.

The TeraScan platform has been designed for production reticle inspection of 248nm and 193nm wavelength reticles for the 90nm node and the 65nm node including typical binary (COG), EPSM, and dark field alternating PSM. Capability extensions are in development for more aggressive RET, such as tri-tone, chromeless, etc. Finally, the system can likely be used for the development of 157nm wavelength and EUV reticles for lithography below the 65nm node.

### 3. TECHNOLOGY

#### 3.1. Image Acquisition

A simple block diagram of the DUV TeraScan image acquisition subsystem is shown in Figure 3-1. It uses a high resolution microscope and linear sensor architecture, as opposed to the multi-beam laser scanner architecture of the current generation UV TeraStar system. The TeraScan architecture offers several advantages to the laser scanner which include the potential for higher speed in the future, and no beam crosstalk.

Referring to the top of the diagram, the illumination source is a 257nm wavelength continuous wave (CW) laser. There is an Active Beam Steering subsystem to compensate for beam drift and to reduce laser replacement time. The Transmitted Illuminator has several different configurations that can be selected by the user at runtime. Two configurations are currently implemented: standard contrast for binary and EPSM reticles, and phase contrast for quartz etch reticles such as alternating, chromeless, etc. The phase contrast mode provides improved imaging contrast to quartz phase defects (bumps and divots) allowing for higher defect sensitivity.

The reticle is inspected with the pattern surface down. The air bearing stage scans the reticle in one axis for continuous image pick-up, and then indexes in the other axis after each swath to provide a serpentine inspection path.

The custom designed objective images the reticle surface through the zoom lens onto the imaging sensor. The zoom lens allows different pixel sizes to be selected by the user at runtime, thus providing different defect sensitivities and associated scan times - currently a 125nm pixel size is available, and now, a 90nm pixel is also available. Image pick-up is done with a time-domain-integration (TDI) sensor. This sensor design offers high speed continuous image pick-up at much lower light levels than a conventional CCD linear sensor.

The system also includes a reflected illumination optical path which is currently used during defect review to aid in the correct classification of contamination. Further, inspection with reflected illumination is also now available for die-to-die mode, while reflected illumination inspection in the die-to-database and STARlight modes is in development

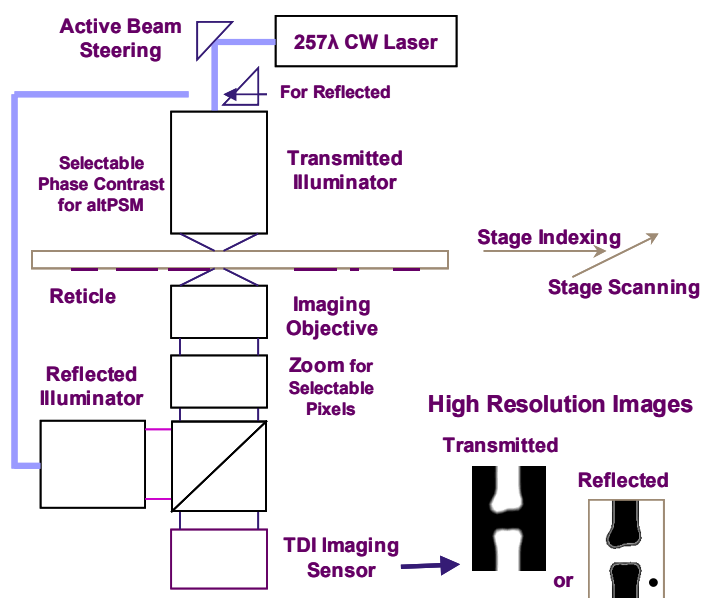


Figure 3-1: TeraScan High Resolution Image Acquisition Subsystem Block Diagram

At the bottom of Figure 3-1, the high resolution images show transmitted and reflected images of a binary reticle. Note that the sub-resolution clear serifs are fully imaged and clearly visible, thus allowing defects on the serifs to be readily detected directly. An oversize clear serif defect is present and visible in both the transmitted and the reflected images, however, a particle on the dark material is also present but is only visible in the reflected light image (dark spot).

As with lithography systems, slight amounts of mechanical or optical error will reduce overall system performance. Since high sensitivity die-to-database inspection is the most demanding of the three applications, the optical and

mechanical tolerances of the platform are determined by this mode. All models are designed with the very tight tolerances required for die-to-database mode, so die-to-die models can be readily upgraded to die-to-database capability.

### 3.2. Image Processing

Figure 3-2 shows a simple block diagram of the TeraScan image processing subsystem. The Tera Image Supercomputer is a fully programmable and scalable multi-processor architecture. This image computer is very similar to the TeraStar image computer but can be configured with more processors and memory for additional speed and algorithm complexity.

The transmitted or reflected image stream is stored in the Optical Image Memory; several swaths are buffered to allow variable processing rates according to geometry density, thus improving the overall speed. Sophisticated alignment and detection algorithms are executed in the Defect Detection block to provide both high sensitivity and binning by defect type and significance. The basic detection method is to overlay a test image with a matching reference image and identify differences above a pre-selected size - any differences are the result of a defect.

For die-to-die inspection, the test and reference images compared are from adjacent die; for die-to-database inspection, the reference image is reconstructed from the database. For STARlight inspection, the transmitted and reflected images of the same geometry are compared.

In Figure 3-2, note that the test Transmitted Image and the reference Modeled image are the same except for the oversize serif (test and reference are shown side-by-side in the operator monitor window). Thus, in the difference image (overlay), everything matches except the oversize serif, which is represented as a bright spot that the defect detectors can readily identify.

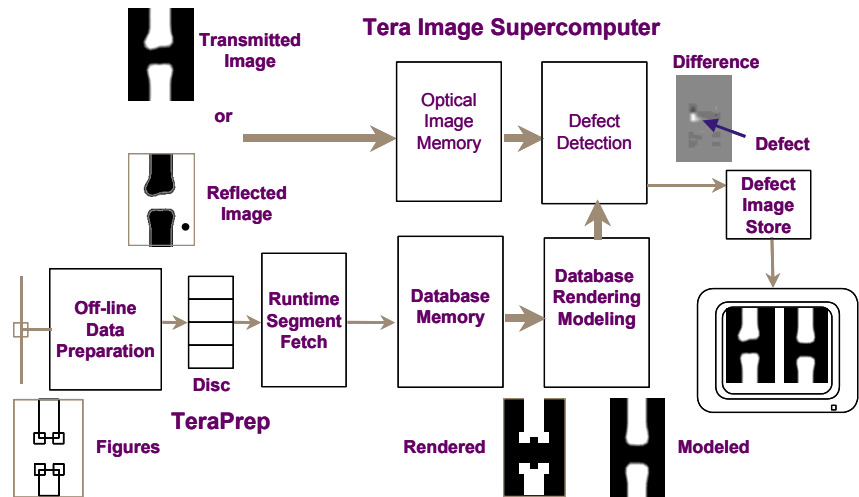


Figure 3-2: TeraScan Image Processing Block Diagram

The processing blocks for die-to-database inspection are shown in the lower part of Figure 3-2. These processing blocks construct an image which will match the optical image. The database image is reconstructed in real time from the database used to write the reticle. Starting from the left side of Figure 3-2, an off-line data preparation operation is performed to optimally organize and format the input database figures for inspection (rather than for design or writing). This step is done off-line and the inspection-ready file is stored on the high speed disc. At runtime, as the optical system is scanning the reticle, the Runtime Segment Fetch block selectively accesses the appropriate figure segments of the database for the current swath and stores them in the Database Memory. As each geometry is processed for defect detection, the database figures are rendered (figures placed in the correct locations and interior lines removed), and then modeled to match the optical image. Sophisticated modeling algorithms are used to ensure that that database image exactly matches the optical image - any error reduces defect detection sensitivity.

These database processing blocks are basically the same as for the current TeraStar system, however, TeraScan can be configured with additional processing speed and capacity for the anticipated larger databases of the advanced nodes. Moreover, TeraScan has more sophisticated modeling capability to provide high sensitivity for the more aggressive OPC and phase shifting designs of the advanced nodes. TeraScan further can be configured with a higher speed Runtime Segment Fetch block to speed the processing of large, high density databases.

### 3.3. Image Acquisition Cut-away

A cut-away illustration of the Image Acquisition Subsystem (IAS) is shown in Figure 3-3. In addition (not shown), there is a separate utilities module (must be located nearby), image computer electronics rack, and data preparation electronics rack (both racks can be remotely located).

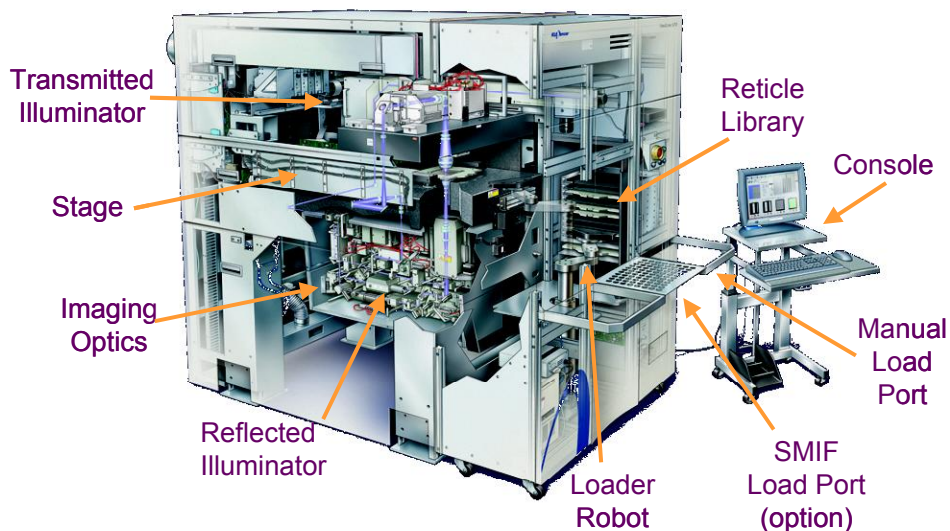


Figure 3-3: TeraScan Image Acquisition Subsystem Cut-away

Referring to Figure 3-3, the Stage is in the middle, the Transmitted Illuminator is above, while the Optics Bench is below (contains the objective, zoom, sensor, and reflected illuminator). Reticles are loaded and unloaded from the front via either a Manual Load Port for unboxed reticles, or the Reticle SMIF Pod (RSP) Load Port (both can be installed simultaneously). A reticle library is included inside for queued operation. The stand-alone operator console can be located nearby.

## 4. TEST RESULTS

The TeraScan 576 die-to-database system recently completed 8 months of internal testing and tuning (August 2003 through March 2004) prior to the start of Beta testing. The 8 months of internal testing consisted of Engineering Test and Alpha Test. Three prototype systems were used for the testing to allow for early assessment of system-to-system variation. Both the 125nm pixel and the new 90nm pixel were used in both transmitted illumination and reflected illumination.

KLA-Tencor uses four standard reticle designs for sensitivity and false detection testing. Selected performance data from these four reticle types is shown in the sections below.

In addition to the standard reticles, KLA-Tencor received approximately fifty-five (55) reticles from the industry to include in the testing; the reticles included a variety of RET types, writer types, manufacturers, geometry designs, and defect types. These reticles were from the 90nm through the 65nm node, primarily for 193 wavelength lithography (some 248nm), and included: binary, 6% EPSM, and dark field alternating PSM. Of the total, approximately thirty (30) were critical product layers, while approximately twenty (20) included programmed defects.

Overall, the testing showed that the system met its target performance level for sensitivity, inspectability, and false detections with no major issues - some minor issues were identified and are being corrected.

#### 4.1. Die-to-database Results for 125nm Pixel and KLA-Tencor Test Reticles

Figure 4-1 shows the sensitivity performance in die-to-database mode using the KLA-Tencor Spica-400-193 test reticle. This test reticle is standard 6% EPSM for 193 lithography and includes a typical Semi-wire programmed defect test section with approximately 430nm dark lines (shown). This result was taken from a prototype system using the 125nm pixel with transmitted illumination and the standard high resolution detectors set at maximum sensitivity (HiRes1 and HiRes2). Each gray box indicates 100% detection from 20 contiguous inspections. The upper number in the gray box is the defect size using the KLA-Tencor maximum inscribed circle (MIC) sizing method using SEM images. The lower number is the detection percentage. The red line indicates the specified performance level which was met by the system. Similar results were obtained using the binary version of this test reticle (data not shown). Also, very little system-to-system, reticle-to-reticle, and day-to-day variation was observed (data not shown).

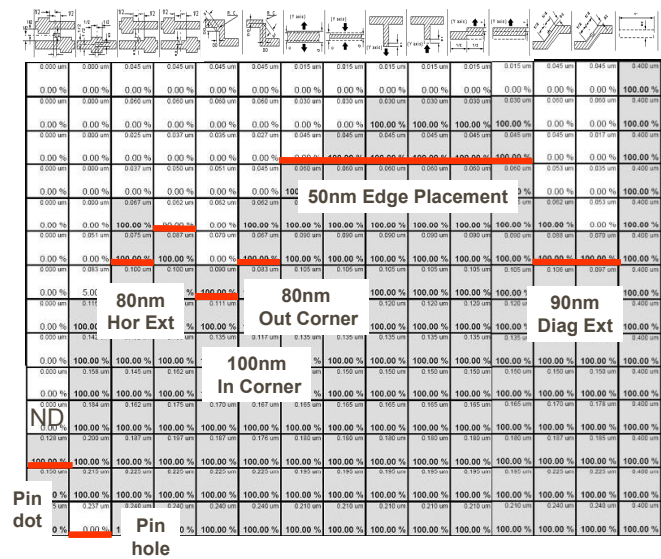


Figure 4-1: Die-to-database sensitivity from Spica-400-193 6% EPSM semi-wire pattern with 125nm pixel transmitted illumination

Figure 4-2 shows the defect images from defect G4 of a typical die-to-database Spica-400-193 inspection (125nm pixel transmitted illumination). Defect G4 is a 60nm undersize CD defect. The gray scale Test and Reference images are shown with the edge enhance feature enabled (green and magenta feature outlines). Note that this defect cannot be correctly classified by simply visually comparing the Test and Reference images since the slight difference is very difficult to discern, whereas, the defect is easily visible in the Difference Image as the dark outline (mismatch between Test and Reference). The operator can further measure the defect using the Linewidth Measuring review tool (not shown).

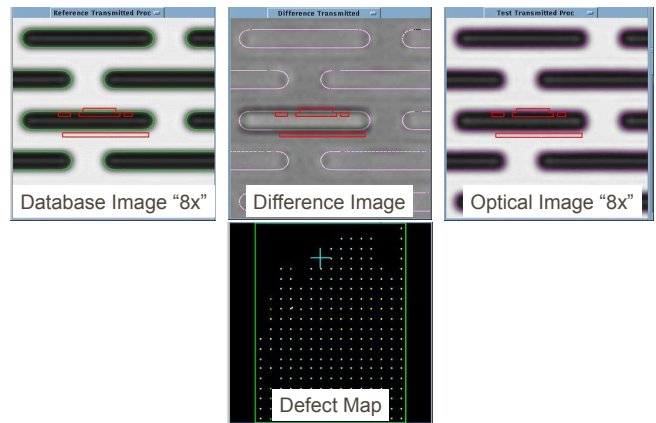


Figure 4-2: 60nm undersize CD defect from Spica-400-193

Note that the difference image is a very uniform gray tone away from the defect, thus, indicating very good matching between the database image and the optical image. This good matching is the result of excellent rendering, modeling, alignment, and compensation algorithms which reconstruct the database image and then exactly match it to the optical image.

The inspection map is also shown where each colored dot is a detected defect. Note that there are no off-grid detections indicating low false detections and, also, a good reticle manufacturing process that produced a very low population of naturally occurring defects.

Considering contact layer defect detection performance, Figure 4-3 shows the contact area defect sensitivity performance of the 125 pixel in the die-to-database transmitted illumination mode using the Cetus-600-193 6% EPSM test reticle and the Litho2 detector. This reticle has programmed oversized and undersized contacts from approximately 1% to 30% area error as measured from a SEM image (not all defects are shown). The nominal contact size is 600nm in both the dense (1:3) and isolated arrays. This particular test was done with the high sensitivity flux detector (Litho2) and shows the specified 6.5% area undersize and 8% area oversize performance (red lines). The Litho2 detector measures "flux" error compared to the database using a simple lithographic method; flux error more closely matches lithographic performance than SEM area error.



Figure 4-3: Die-to-database contact flux sensitivity with 125nm pixel transmitted illumination from Cetus-600-193

Figure 4-4 shows an undersized contact detected in die-to-database mode from the Cetus-600-193 test reticle (600nm nominal contact diameter). This particular programmed defect measures approximately 100nm CD error (diameter), and measures 25% area error by SEM. This amount of error is easily visible visually when comparing the database image with the optical image, as well as in the difference image. When measuring flux using the Litho2 lithographic detector, this defect measures a 60% flux error indicating a highly printable defect.

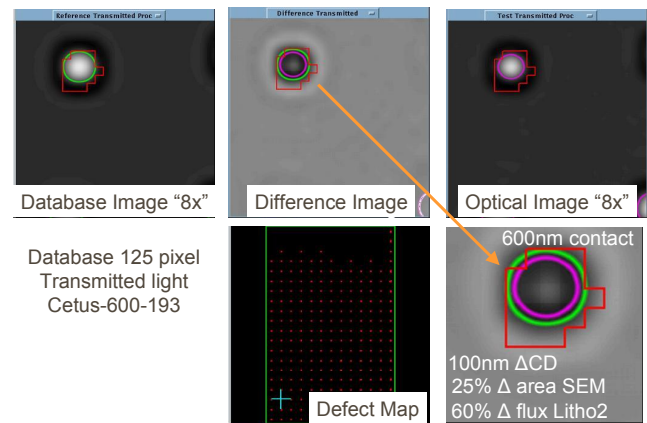


Figure 4-4: 100nm undersized contact detected by Litho2 in die-to-database mode with 125nm pixel transmitted illumination

Figure 4-5 shows three undersized contacts from the Cetus-600-193 test reticle. They are sized with CD error of 100nm, 40nm, and 20nm respectively, and are shown along with their corresponding SEM area error and Litho2 flux error measurements. Note that the smallest undersize contact (rightmost) produces just a 6% area error and is very difficult to discern visually, thus requiring careful defect disposition using the measurements of the Litho2 detector along with the other review measurement tools available.

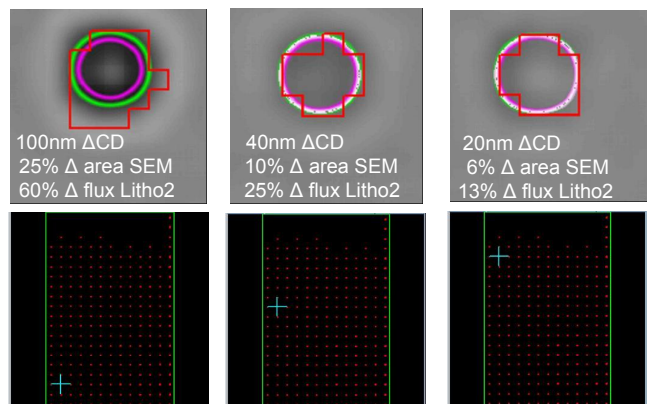


Figure 4-5: 100nm, 40nm, and 20nm undersized contacts detected by Litho2 in die-to-database mode with 125nm pixel transmitted illumination

Considering alternating PSM defect detection performance, Figure 4-6 shows typical die-to-database quartz edge bump defect detection performance with the 125nm pixel using standard optical contrast and focus in transmitted illumination. The Dione-280-193 AltPSM test reticle is used. This test reticle is a dark field alternating design with 280nm dark linewidths and an etch depth suitable for 193 lithography. The reticle contains quartz edge bump defects located in a 180° well, along with a selection of chrome defects (not shown). The edge bump type of quartz defect is typically the most lithographically significant quartz type. The defect sizes are determined using the KLA-Tencor MIC method from SEM images. The gray squares are 100% detection (20 inspections); the red line indicates the specified performance (180nm for 180° edge bumps). Note that none of the 120° and 60° defects included on this test reticle are detected 100%, so these are not specified.

180°	0.042 um	0.071 um	0.069 um	0.100 um	0.121 um	0.113 um	0.138 um	0.160 um	0.183 um	0.196 um	0.213 um	0.221 um	0.221 um	0.263 um	0.288 um	0.304 um	0.300 um
	0.00 %	0.00 %	0.00 %	0.00 %	100.00 %	80.00 %	100.00 %	100.00 %	100.00 %	100.00 %	100.00 %	100.00 %	100.00 %	100.00 %	100.00 %	100.00 %	100.00 %
120°	0.025 um	0.017 um	0.042 um	0.029 um	0.058 um	0.063 um	0.000 um	0.292 um									
	0.00 %	0.00 %	0.00 %	0.00 %	0.00 %	0.00 %	0.00 %	0.00 %	0.00 %	0.00 %	0.00 %	0.00 %	0.00 %	0.00 %	0.00 %	65.00 %	85.00 %
60°	0.025 um	0.038 um	0.050 um	0.050 um	0.090 um	0.096 um	0.121 um	0.129 um	0.154 um	0.169 um	0.223 um	0.228 um	0.254 um	0.263 um	0.263 um	0.304 um	0.288 um
	0.00 %	0.00 %	0.00 %	0.00 %	0.00 %	0.00 %	0.00 %	0.00 %	0.00 %	0.00 %	0.00 %	0.00 %	0.00 %	0.00 %	0.00 %	5.00 %	0.00 %

Figure 4-6: Quartz edge bump defects detected in die-to-database mode with 125 pixel standard contrast transmitted light - Dione-280-193 test reticle

To improve quartz defect sensitivity, KLA-Tencor developed phase contrast imaging which is currently available only for the die-to-die mode (TeraPhase 501). The significant improvement in quartz defect imaging is illustrated in Figure 4-7, which shows a 183nm quartz edge bump (SEM measured) which is imaged with standard contrast and focus (left), versus the same defect imaged with phase contrast and off-focus (right). There is a significant improvement in the visibility of the quartz defect when using phase contrast, which means that defect detection is significantly improved. While phase contrast illumination is currently available in the die-to-die mode only (TeraPhase 501); KLA-Tencor is currently investigating the modeling algorithms necessary to support phase contrast illumination in the die-to-database mode as a possible future capability.

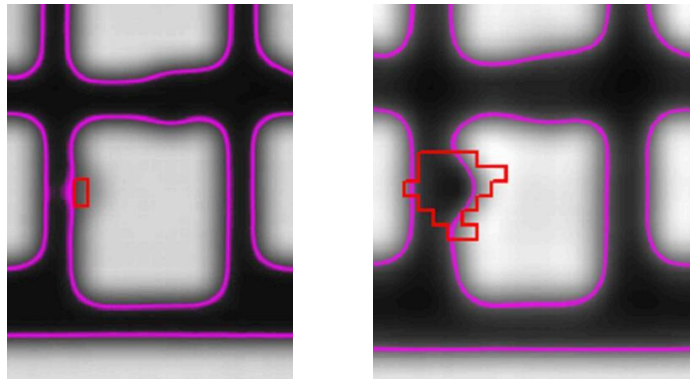


Figure 4-7: 183nm quartz edge bump imaged in standard contrast illumination (left) versus phase contrast illumination (right).

For comparison, Figure 4-8 shows the quartz edge bump defect performance available in the die-to-die mode when using phase contrast illumination (TeraPhase 501). Note the significant improvement in the detection of all three defect phases (180°, 120°, 60°). The specified performance is indicated by the red lines.

180°	0.042 um	0.071 um	0.069 um	0.100 um	0.121 um	0.113 um	0.138 um	0.160 um	0.183 um	0.196 um	0.213 um	0.221 um	0.221 um	0.263 um	0.288 um	0.304 um	0.300 um
	0.00 %	100.00 %	100.00 %	100.00 %	100.00 %	100.00 %	100.00 %	100.00 %	100.00 %	100.00 %	100.00 %	100.00 %	100.00 %	100.00 %	100.00 %	100.00 %	100.00 %
120°	0.025 um	0.017 um	0.042 um	0.029 um	0.058 um	0.063 um	0.000 um	0.292 um									
	0.00 %	0.00 %	0.00 %	0.00 %	15.00 %	5.00 %	100.00 %	100.00 %	100.00 %	100.00 %	100.00 %	100.00 %	100.00 %	100.00 %	100.00 %	100.00 %	100.00 %
60°	0.025 um	0.038 um	0.050 um	0.050 um	0.090 um	0.096 um	0.121 um	0.129 um	0.154 um	0.169 um	0.223 um	0.228 um	0.254 um	0.263 um	0.263 um	0.304 um	0.288 um
	0.00 %	0.00 %	0.00 %	0.00 %	0.00 %	90.00 %	100.00 %	100.00 %	100.00 %	100.00 %	100.00 %	100.00 %	100.00 %	100.00 %	100.00 %	100.00 %	100.00 %

Figure 4-8: Quartz edge bump defects detected in die-to-die mode with 125nm pixel phase contrast transmitted light - Dione-280-193 test reticle

Considering the more sensitivity 90nm pixel, Figure 4-9 shows the higher sensitivity achieved with the smaller 90nm pixel. Approximately 20% higher sensitivity is achieved as shown with the Spica-400-193 test reticle. Since the 90nm pixel is intended for 65nm node reticles, smaller linewidth and contact size versions of the Spica and Cetus reticles are currently being qualified to give a better representation of the system performance for 65nm node reticles. The defects are labeled with column A being the leftmost, and row 1 being the topmost.

Figure 4-10 below shows Spica defect G3 which is a 45nm undersize CD defect as detected by the 90nm pixel (Spica-400-193). Note also that this difference image shows little noise indicating very good matching between the optical side and the database side. Good matching is the result of very good rendering and modeling of the input database, as well as minimal residual imaging errors on the optical side. In the defect map, there are a number of off-grid defects detected as compared to the 125nm pixel - these are small naturally occurring defects that are detected by the higher sensitivity of the 90nm pixel. The population of naturally occurring defects needs to be carefully controlled otherwise the sensitivity results can become inaccurate due to off-grid defects being grouped with the on-grid defects.

#### 4.2. Testing with Industry Provided Reticles

As discussed previously, fifty-five advanced reticles were provided by twelve reticle manufacturers and were used to further test the system to assess real-world performance. Results from a selection of these reticles are shown below. In these examples, a "false detection" is a detection that is caused by the inspection system such as due to vibration, residual optical distortion, mis-alignment, a hardware or software problem, etc. Small real defects that the user may not want to be detected are not counted as "false". Also, a detector is operating at maximum sensitivity with a setting of 100 - lower settings mean reduced sensitivity.

Figure 4-11 shows a die-to-database comparison between the current generation UV wavelength TeraStar F87HR using its smallest 150nm pixel, and the new DUV TeraScan 576 using the 125nm pixel in transmitted illumination. This reticle is a 90nm node 6% EPSM line/space layer for 193 lithography with an aggressive OPC design using corner serifs and dark assist lines. The very small clear spaces between the primary lines and the dark assist lines,

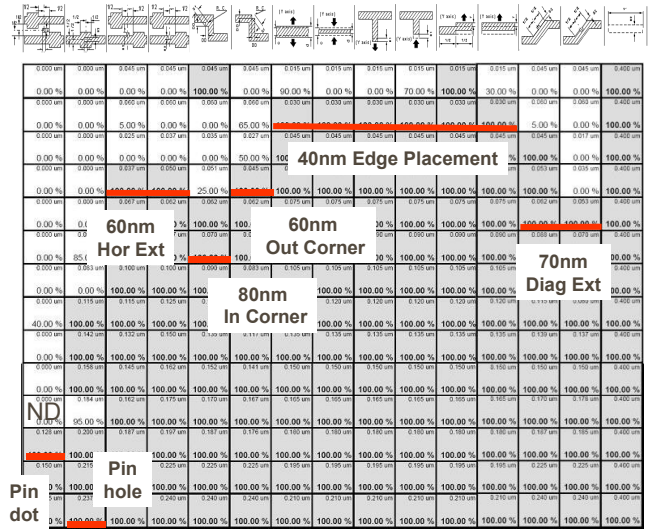


Figure 4-9: 90nm pixel die-to-database sensitivity from Spica-400-193 6% EPSM semi-wire pattern with transmitted illumination

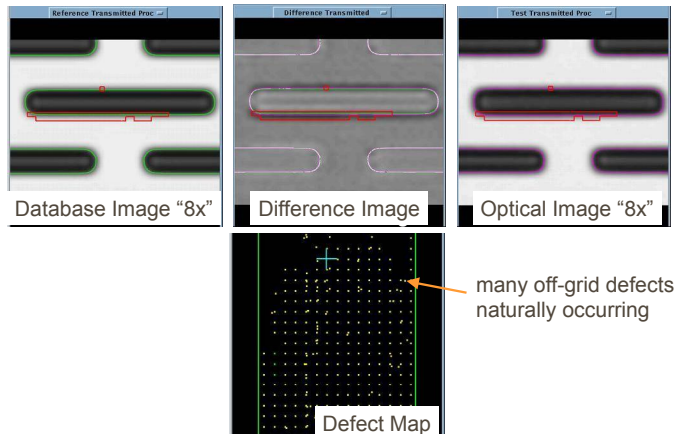


Figure 4-10: 45nm undersize CD Defect from Spica-400-193

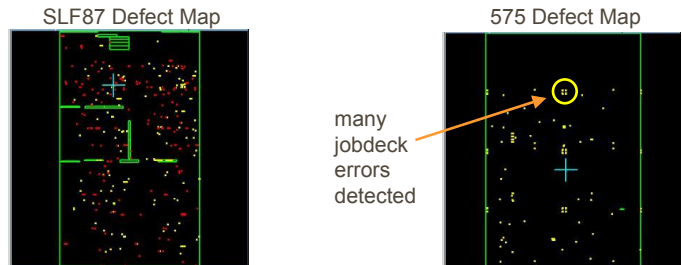


Figure 4-11: 90nm node 6% EPSM 193 product reticle showing high false detection count with the F87HR, and low false detections with the 576 using the 125nm pixel

and also between the primary lines and adjacent corner serifs, were very challenging for the F87HR to render and model properly. This caused a high number of bridging type false detections (modeling failure), and required reduced detector settings which limited overall defect detection performance. The defect map on the left of Figure 4-11 shows a typical inspection with a high count of false detections (920) even though the detectors were reduced (in production, the detectors are reduced further to manage the total number of detections).

When inspected with the 576, high detector settings were used which provided high sensitivity, and there were low false detections (no evidence of bridging). The defect map on the right in Figure 4-11 shows a typical inspection. This inspection also revealed a high number of job-deck errors that were not detected by the F87HR; these job deck errors were erroneous small gaps between adjacent figures.

Figure 4-12 shows another 90nm node 6% EPSM 193 line/space reticle inspected in die-to-database mode using the 576 125nm pixel transmitted illumination. This was a large area inspection using nearly the maximum detector settings to achieve maximum sensitivity with the high resolution detectors (100.100.95-100). The inspection resulted in 26 total detections with no false detections. A small dark extension defect (~30nm) is shown. In this example, two regions containing chrome were covered by DNIR (Do Not Inspect Region) to eliminate false detections or reduced sensitivity caused by the chrome. KLA-Tencor is currently developing the capability to inspect chrome regions on EPSM in a single pass (tri-tone die-to-database mode).

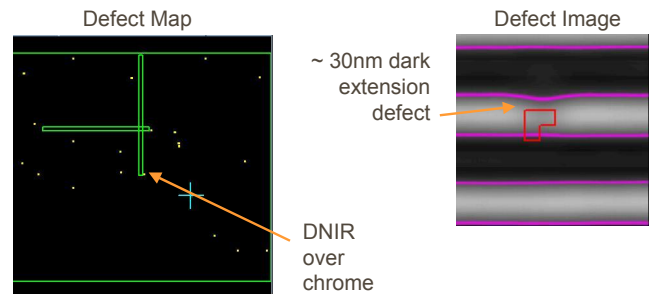


Figure 4-12: 125nm pixel die-to-database inspection of 90nm node 6% EPSM 193 line/space layer showing ~30nm dark extension defect

Figure 4-13 shows a 90nm node 6% EPSM 193 hole layer inspected in die-to-database mode with the 125nm pixel in transmitted illumination. This was a full area inspection using the maximum detector settings (100.100.100-100) to achieve the maximum possible sensitivity with the high resolution detectors; additional sensitivity could be achieved by also using the Litho2 detector. The inspection resulted in 20 total detections with no false detections. A small dark extension defect (~30nm) is shown; it corresponds to about a 20% flux error.

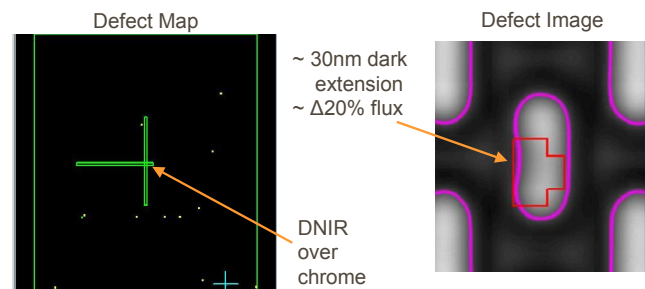


Figure 4-13: 125nm pixel die-to-database inspection of 90nm node 6% EPSM 193 hole layer showing ~30nm dark extension defect (~20% flux error)

Figure 4-14 shows a 90nm node dark field 193 alternating PSM line/space layer inspected in die-to-database mode with the 125nm pixel in transmitted illumination. This inspection used the chrome layer database only so the reconstructed database didn't know which areas were 180° and which were 0°. Since there are slight differences in the optical image between the 180° regions and the 0° degree regions, this differences causes some errors to occur between the database image and the optical image, thus resulting in slightly reduced detector settings (85.85.85-100). The inspection resulted in 23 total detections with no false detections. A small quartz bridge defect is shown.

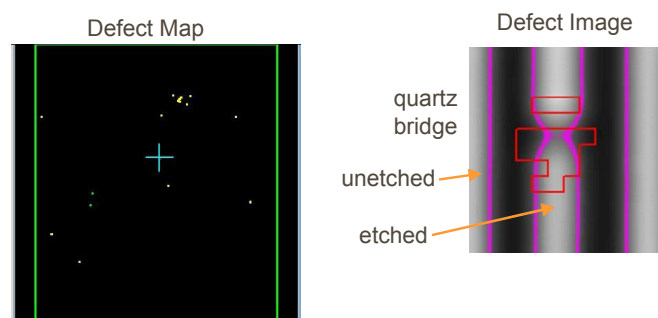


Figure 4-14: 125nm pixel die-to-database inspection of 90nm node 193 dark field alternating PSM line/space layer showing quartz bridge defect.

Considering the 90nm pixel and 65nm node reticles, Figure 4-15 shows a 65nm node 6% EPSM 193 lithography line/space layer inspected in die-to-database mode with the 90nm pixel in transmitted illumination. A full area inspection was completed but required reduced detector settings (80.80.80-100) due to a high population of small, naturally occurring defects that are detected by the very sensitive 90nm pixel. At this detector setting, there were 152 total detections with low false detections. A small dark extension defect is shown (~30nm) which is about 10% of the linewidth.

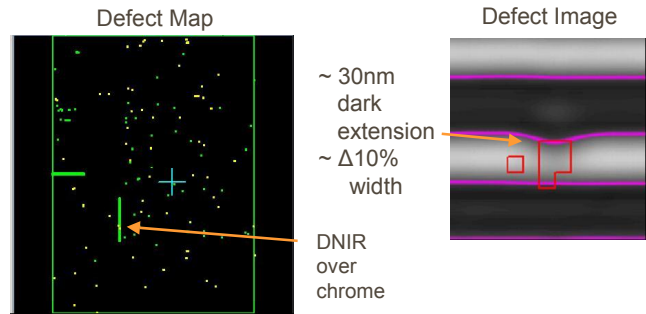


Figure 4-15: 90nm pixel die-to-database inspection of 65nm node 6% EPSM 193 line/space layer showing ~30nm dark extension defect (~10% of the linewidth)

Another example of a 65nm node 6% EPSM 193 line/space reticle is shown in Figure 4-16. This reticle was inspected with the 90nm pixel in die-to-database mode using transmitted illumination at reduced detector settings (85.85.85-100). The reduced settings were required due to a high population of small real defects detected by the very sensitive 90nm pixel. At this detector setting, there were 25 total detections with low false detections. A dark extension defect is shown (~90nm) which is about 25% of the linewidth.

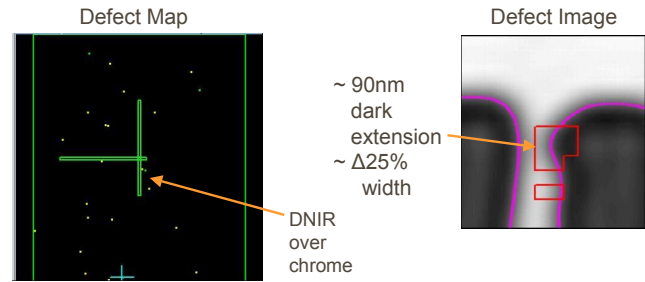


Figure 4-16: 90nm pixel die-to-database inspection of 65nm node 6% EPSM 193 line/space layer showing ~90nm dark extension defect (~25% of the linewidth)

Figure 4-17 shows a 65nm node dark field 193 alternating PSM line/space layer inspected in die-to-database mode with the 90nm pixel in transmitted illumination. The inspection was done with reduced detector settings (80.80.80-80) to avoid a high count of small real defects. The inspection resulted in 278 total detections with low false detections. A small quartz bridge defect is shown.

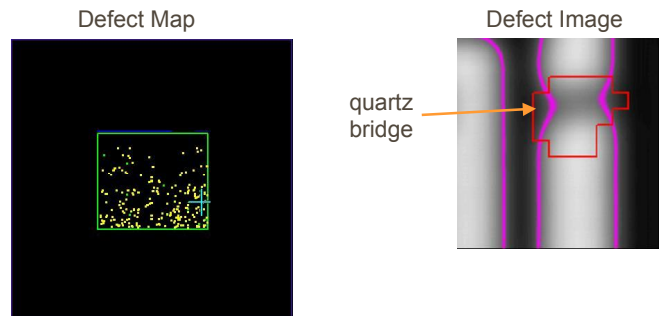


Figure 4-17: 90nm pixel die-to-database inspection of 65nm node 193 dark field alternating PSM line/space layer showing quartz bridge defect.

Figure 4-18 shows another 65nm node dark field 193 alternating PSM line/space layer inspected in die-to-database mode with the 90nm pixel in transmitted illumination. The inspection was done with reduced detector settings (60.60.60-90) to avoid a high count of small real defects and the mismatch that occurs when using only the chrome layer for the database image. The inspection resulted in 206 total detections with low false detections. A small quartz edge bump defect on a narrow line is shown.

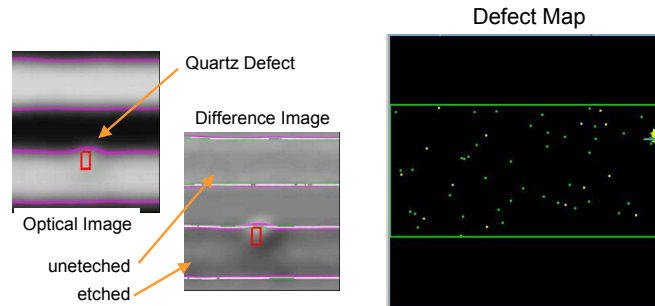


Figure 4-18: 90nm pixel die-to-database inspection of 65nm node 193 dark field alternating PSM line/space layer showing quartz edge defect.

### 4.3. Observations from Industry Provided Reticles

Testing from the fifty-five reticles provided by the industry revealed the following about the system:

1. Low false detections - during the alpha test period, there were very few false detections observed even though high sensitivity settings were used and large area inspections were performed on reticles with complex OPC and advanced PSM. This result indicates that the system has excellent rendering and modeling algorithms so the reconstructed database image closely matches the optical image, and further that the optical image is of high quality minimizing errors due to vibration, optical distortion, etc. Furthermore, there were very few misalignment false detections indicating excellent alignment and compensation algorithms.
2. High sensitivity - the KLA-Tencor programmed defect test reticles revealed high sensitivity to the standard defect and geometry types and sizes. The industry also provided programmed defect test reticles which showed high sensitivity to a wider variety of defect types, geometry types, and geometry sizes than the KT standard reticles (results not shown). Reticles manufactured with state-of-the-art methods typically allowed high sensitivity and had minimal small real defects. The 90nm pixel appeared to be more sensitive than the current manufacturing methods could support, indicating that 65nm manufacturing methods in the future will likely be improved.
3. Full speed - although no results were shown in this paper, the system showed acceptable data preparation speed for the large files typical of 90nm and 65nm node reticles, and few runtime slowdowns due to data density. This is the result of multiple processors being used for data preparation, and the speed improvements to the Runtime Segment Fetch function compared with the current TeraStar system.

### 4.4. Reflected Illumination Test Results

Another recent capability not previously reported, is inspection in die-to-die mode using reflected illumination rather than the traditional transmitted illumination. Reflected illumination is valuable for the detection of contamination defects in the dark areas of the reticle where they cannot be readily seen by transmitted illumination. Furthermore, certain types of PSM defects can be more visible in reflected illumination as compared to transmitted illumination, thus allowing higher defect sensitivity. Discussed below is one type of EPSM defect, pinholes, that are much more detectable in reflected illumination.

Figure 4-19 shows a 200nm pinhole defect on a 6% EPSM 193 reticle (Spica-400-193) as imaged using

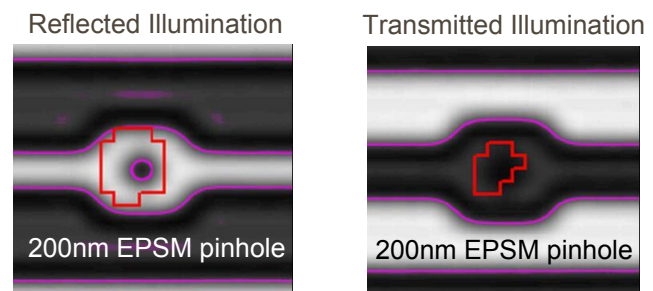


Figure 4-19: 200nm pinhole defect on 6% EPSM 193 reticle showing high visibility in reflected illumination versus low visibility in transmitted illumination (125R pixel)

reflected illumination (left) and also transmitted illumination (right). The pinhole has limited visibility in transmitted illumination, and thus is not easily detected, whereas, it is highly visible in reflected illumination and therefore easily detected.

The sensitivity performance of the reflected light die-to-die mode is similar to transmitted light with the exception of much better pinhole performance, slightly better performance on some of the clear defects, and slightly worse performance on some of the dark defects. A typical sensitivity chart is shown in Figure 4-20.

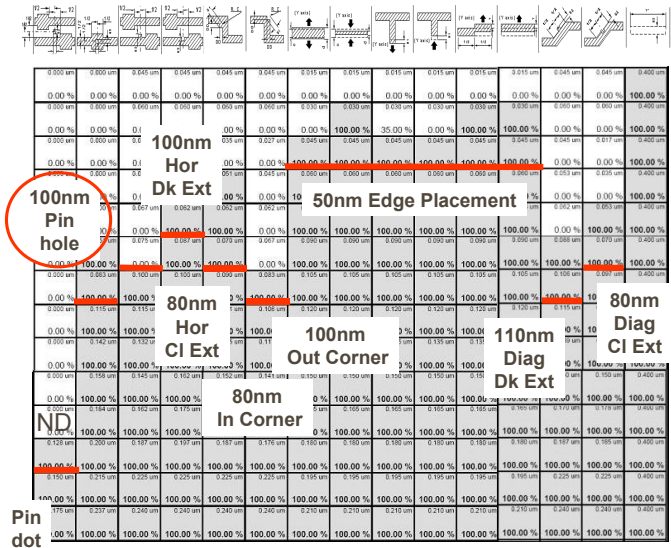


Figure 4-20: Reflected illumination die-to-die sensitivity from Spica-400-193 6% EPSM semi-wire pattern with 125R pixel showing improved pinhole sensitivity

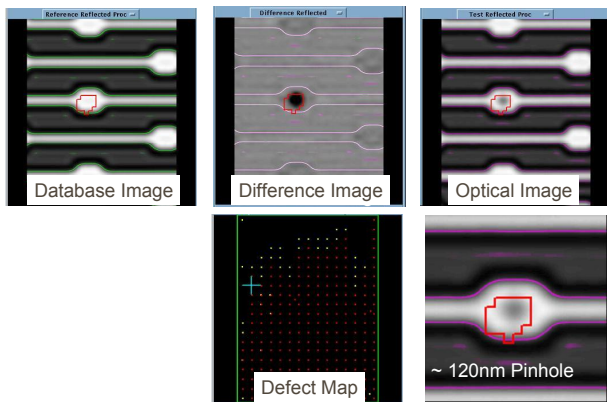


Figure 4-21: Die-to-database reflected illumination example on Spica-400-193 6% EPSM semi-wire pattern with 125R pixel showing improved pinhole sensitivity.

Figure 4-22 shows a 90nm node 6% EPSM 193 metal layer being inspected in die-to-database mode 125R pixel using reflected illumination and high detector settings (90.90.90-90). The inspection had high sensitivity and low false detections. A contamination defect is shown that is located very close to a geometry edge where it could have an impact on the lithographic performance.

KLA-Tencor is currently developing the capability to inspect in die-to-database mode with reflected illumination. Figure 4-21 shows a 120nm pinhole being detected on the Spica-400-193 6% EPSM 193 test reticle in die-to-database reflected illumination mode. Note that the difference image shows very little noise suggesting a good database model for the reflected imaging, and the defect map shows no false detections.

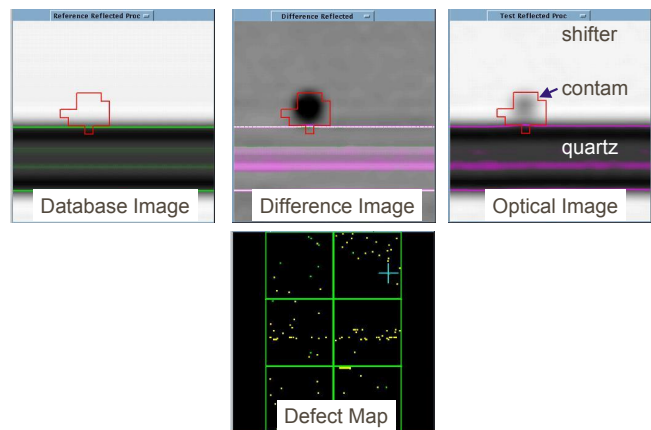


Figure 4-22: Die-to-database reflected illumination example on 90nm node 6% EPSM 193 metal layer with 125R pixel showing contamination defect on dark near an edge

## 5. CONCLUSIONS

A new DUV die-to-database high-resolution reticle defect inspection platform has been developed. This platform is designed to meet the 90nm through 65nm node 248/193nm lithography reticle qualification requirements of the IC industry. Three prototype systems with the previous 125nm pixel, and the new 90nm pixel have been tested in die-to-database mode using approximately fifty-five advanced reticles provided by the industry. These reticles represent the 90nm node through the 65nm node. They included COG, EPSM, and altPSM types, with various OPC styles (serif, jog, and SRAF). Programmed defect types and regular full field product reticles were inspected. Data from the testing showed that the system met its high sensitivity and low false detection targets - selected supporting data was shown in this paper.

The shorter wavelength, smaller pixel size, and improved rendering and modeling algorithms of the TeraScan system showed significant improvements in inspection capability of aggressive OPC versus the current UV TeraStar system. In addition, a new reflected light capability was tested in die-to-die mode, along with early results for the die-to-database mode. The reflected light mode showed significant improvement in pinhole sensitivity for EPSM material versus transmitted illumination, as well as the ability to find contamination in dark areas of the reticle.

While not discussed in this paper, the system also includes die-to-database versions of the lithography oriented detectors introduced last year for the die-to-die mode. These detectors are designed to provide high sensitivity to those defects that are likely to have lithographic significance, while providing lower sensitivity to those defects with likely little lithographic significance. When used in conjunction with the traditional high resolution detectors, the user can readily identify those defects with likely lithographic significance requiring repair, and those defects that are likely not lithographically significant but still important for reticle process monitoring and improvement (typically not repaired).

The TeraScan platform includes several inspection modes, including die-to-die (discussed previously), die-to-database mode (discussed in this paper), reflected light mode (partly discussed in this paper), and STARlight mode (in development).

## 6. FUTURE WORK

There are several new capabilities which are currently in development for the TeraScan platform. Future work will include testing these capabilities. They include:

- Smaller linewidth and contact size test reticles for the 65nm node
- Reflected illumination die-to-database mode
- Tri-tone die-to-database mode
- STARlight mode

## ACKNOWLEDGEMENTS

The authors thank the many individuals and organizations that contributed to the development and testing of the TeraScan 576, including:

- International SEMATECH for Tera Family and AltPSM funding
- Worldwide reticle manufacturers and fabs for providing reticles used in development and testing
- KLA-Tencor RAPID Applications Team for data collection and analysis
- KLA-Tencor TeraScan Development Team for platform development

## REFERENCES

W. Broadbent, et al, "Results from a new reticle defect inspection platform", *23rd Annual BACUS Symposium on Photomask Technology*, Kurt R. Kimmel, ed., Proc SPIE Vol 5256, p. 474-488, 2003